Journal of Hydrology 373 (2009) 96–102

Contents lists available at ScienceDirect

Journal of Hydrology

journal homepage: www.elsevier.com/locate/jhydrol

Effects of mechanical dispersion on the morphological evolution of a chemical dissolution front in a fluid-saturated porous medium

Jui-Sheng Chen [a,*], Chen-Wuing Liu [b], Geng-Xin Lai [a], Chuen-Fa Ni [a]

[a] Graduate Institute of Applied Geology, National Central University, Taoyuan 32001, Taiwan, ROC
[b] Department of Bioenvironmental Systems Engineering, National Taiwan University, Taipei 10617, Taiwan, ROC

ARTICLE INFO

Article history:
Received 7 October 2008
Received in revised form 13 April 2009
Accepted 16 April 2009

This manuscript was handled by L. Charlet, Editor-in-Chief, with the assistance of Carlos Ayora, Associate Editor

Keywords:
Chemical dissolution front
Wormhole
Mechanical dispersion
Planar front
Single-fingering front
Double-fingering front

SUMMARY

The dissolution-induced finger or wormhole patterns in porous medium or fracture rock play a crucial role in a variety of scientific, industrial, and engineering practices. Although previous studies have extensively presented a number of numerical models which couples a system of nonlinear governing equations of porosity change due to mineral dissolution, the conservations of groundwater flow and transport of chemical species to investigate the morphological pattern of a chemical dissolution front within a fluid-saturated porous medium, whereas the mechanical dispersion effect has generally been neglected in the model development. This study addresses the effects of mechanical dispersion on the morphological evolution of a chemical dissolution front for a variety of cases. Mechanical dispersion processes is incorporated with the coupled nonlinear governing equation system so as to rebuild a newly numerical model. The results of numerical simulations demonstrate that mechanical dispersion has pronounced impacts on the morphological pattern of the chemical dissolution front. For single local non-uniformity case, mechanical dispersion reduces the finger length of an unstable single-fingering front or retains the shape of a stable planar front while speeding up the front advancement. In the case of two local non-uniformities, adding mechanical dispersion with different flow conditions can yield one of the following results: (1) the shape of the stable planar front is maintained but its advancement is accelerated; (2) the shape of the unstable single-fingering front is maintained but its length is reduced; (3) the unstable double-fingering front is merged into an unstable single-fingering front; and (4) the shape of the unstable double-fingering front is preserved but its fingering length is reduced. A comparison between the behavior diagrams of dissolution front morphology (with and without considering mechanical dispersion) shows that the double-fingering front occurs under condition where the upstream pressure gradient is higher and the non-uniformity spacing is larger while mechanical dispersion is taken into consideration.

Introduction

The morphological evolution of a chemical dissolution front within a fluid-saturated porous medium is an important topic in both geological processes and engineering applications such as stimulation of petroleum reservoirs, environmental contaminant transport, mineral mining, geological sequestration of carbon dioxide, chemical weathering, diagenesis, concrete degradation, bioremediation, and dissolution/formation of hydrates. When groundwater enters a solute-saturated porous medium, it dissolves minerals to maintain the equilibrium state of the solution, thereby increasing the medium porosity and ultimately the permeability. If the porosity in some region of the porous medium is slightly higher than that in other region (herein referred to as a local non-uniformity), groundwater will preferentially flows into this highly permeable zone, thus increasing the mineral dissolution rate. An increasing dissolution rate subsequently enhances the local porosity and groundwater flow, typically resulting in an increase of local groundwater flow and dissolution rate. This positive feedback among porosity, groundwater flow and chemical dissolution tends to focus groundwater flow into this local zone and amplify the local non-uniformity into an unstable dissolution fingering front. However, other factors such as molecular diffusion consistently compete with the flow-focusing mechanism, inhibiting the elongation of the unstable dissolution fingering front (e.g., Chadam et al., 1986; Ortoleva et al., 1987a,b; Chen and Ortoleva, 1990; Ortoleva, 1994; Chen and Liu, 2002; Zhao, 2008a,b,c).

Matrix acidizing in petroleum engineering is a commonly used well stimulation technique in which acid is injected into the

* Corresponding author. Address: Graduate Institute of Applied Geology, National Central University, No. 300, Jungda Rd., Jhongli City, Taoyuan 320, Taiwan, ROC. Tel.: +886 3 2807427; fax: +886 3 4263127.
E-mail address: jschen@app.geo.ncu.edu.tw (J.-S. Chen).

0022-1694/$ - see front matter © 2009 Elsevier B.V. All rights reserved.
doi:10.1016/j.jhydrol.2009.04.014

formation in order to dissolve a portion of the rock and hence, recover or enhance the permeability in the near well-bore area. During the dissolution of rock fractures the positive feedback between fluid flow and mineral dissolution can result in the formation of narrow channels called wormholes (Kalia and Balakotaiah, 2009). Several experimental and theoretical studies have been done to understand the wormhole formations (Hofner and Fogler, 1988; Hung et al., 1989; Kalia and Balakotaiah, 2007, 2009).

Chadam et al. (1986) presented a pioneering study in the development of a two-dimensional numerical model, coupling a set of the governing partial differential equations of groundwater flow, chemical species transport and porosity change induced by dissolution in their investigation of morphological patterns of the chemical dissolution front in a homogeneous porous medium with a single local non-uniformity. According to their results, a single local non-uniformity is inhibited into a stable planar front when a low upstream pressure gradient (or inlet velocity) is applied, or grows into an unstable single-fingering front given a high upstream pressure gradient. Following Chadam et al. (1986), extensive research was carried out to provide a deep understanding of chemical dissolution fronts within a fluid-saturated porous medium (Chadam et al., 1986; Chen and Ortoleva, 1990; Ortoleva, 1994; Renerd et al., 1998; Chen and Liu, 2002, 2004; Zhao et al., 2008a–c). Zhao et al. (2008a,b) noticed that some governing equations derived by Chadam et al. (1986) were incorrect due to two conceptual mistakes: including (1) the confusion between the average linear velocity and Darcy velocity for a fluid-saturated medium and (2) the neglect of the dissolved mineral shape, and they re-derived the governing equations to correct those errors. It should also be noted that in all of these studies molecular diffusion was considered solely by assuming a slow groundwater flow, ignoring the mechanical dispersion effect resulting from spatial variations in pore water velocity.

For most groundwater flow problem, molecular diffusion is usually only a factor in the cases of very low pore water velocity such as in tight packed soil or clay; mechanical dispersion generally dominates the species transport process. Therefore, mechanical dispersion might be the primary factor governing the morphological pattern of a chemical dissolution front. Although a considerable amount of research has been conducted into the morphological patterns of a chemical dissolution front within a fluid-saturated porous medium, to the best of the authors' knowledge, little work has been done where mechanical dispersion is taken into consideration. Thus, in this study we aim to investigate the effects of mechanical dispersion on the morphological evolutions of a chemical dissolution front within a fluid-saturated porous medium. We incorporate the mechanical dispersion process into the coupled nonlinear governing equation system so as to rebuild the numerical model describing morphological evolutions of a chemical dissolution front. The newly developed numerical model is then applied to demonstrate how mechanical dispersion affects the morphological evolution of a single local non-uniformity and two local non-uniformities. We also include the behavior diagram of a chemical dissolution front.

Mathematical model

The dynamics of changes in media porosity, groundwater flow and transport of chemical species induced by the mineral dissolution reaction in a fluid-saturated porous medium can be formulated as a set of coupled nonlinear partial differentiation equations. In the following section we describe the coupled equations governing porosity changes affected by the kinetic dissolution reaction, the conservations of the groundwater flow and the transport of chemical species.

Porosity changes due to the kinetic dissolution reaction

Change in pore volume occurs as a result of a reduction in the volume of the solid phase induced by mineral dissolution. The relationship between porosity change and kinetic chemical dissolution can be derived by invoking the conservation of the total volume in porous media. In this study it is assumed that: the porous medium consists of pores, and soluble and insoluble grains; the mineral grains are cubic in shape and occupy a given volume; and the number of mineral grains remains unchanged after mineral dissolution. Moreover, a single solid component in the porous medium such as calcite and a single species in the groundwater such as calcium or carbonate ion are considered. The chemical dissolution reaction follows the first-order kinetics equation. The change in porosity resulting from the kinetic chemical dissolution can thus be expressed as (Zhao et al., 2008b)

$$\frac{\partial \phi}{\partial t} = \Gamma \cdot 6 \cdot n^{1/3}(\phi_f - \phi)^{2/3}(C_{eq} - C) \tag{1}$$

where ϕ is the porosity [dimensionless]; Γ denotes the chemical dissolution reaction rate constant [$M^{-1}L^4T^{-1}$]; n represents the number of mineral grains per unit medium volume [L^{-3}]; C species concentration in the groundwater [ML^{-3}]; ϕ_f the final porosity after complete dissolution of soluble minerals [dimensionless] and C_{eq} is the equilibrium concentration of chemical species in the groundwater [ML^{-3}].

Conservation of groundwater flow

After incorporating Darcy's law into the continuity equation for groundwater flow, the groundwater flow equation can be written as

$$\frac{\partial \phi}{\partial t} = \frac{\partial}{\partial x}\left[\psi(\phi)\frac{\partial p}{\partial x}\right] + \frac{\partial}{\partial y}\left[\psi(\phi)\frac{\partial p}{\partial y}\right] \tag{2}$$

where p denotes the pore-water pressure [$ML^{-1}T^{-2}$]; $\psi(\phi) = \frac{k(\phi)}{\mu}$ [$M^{-1}L^3T$]; $k(\phi)$ the intrinsic permeability [L^2]; and μ is the dynamic viscosity of water [$MT^{-1}L^{-1}$]. A modified form of the Fair–Hatch relation is adopted herein to characterize the dependence of the intrinsic permeability ($k(\phi)$) on porosity (Chadam et al., (1986); Chen and Liu, 2002)

$$k(\phi) = \frac{\phi^3}{E_2[(1-\phi)^{2/3} + E_1(\phi_f - \phi)^{2/3}]^2} \tag{3}$$

where E_1 and E_2 are constants.

Conservation of chemical species transport

To investigate the effects of mechanical dispersion on morphological evolution of a chemical dissolution front, the major transport mechanisms, advection, molecular diffusion and mechanical dispersion are all considered. Fick's law is used to describe both molecular diffusion and mechanical dispersion mass transport flux. The mechanical dispersion coefficient is commonly assumed to be linearly proportional to the average pore water velocity. Besides the above major transport mechanisms, the dissolution reaction will also causes mass transfer from the solid phase into the aqueous phase, thus raising the chemical species concentration in the groundwater. Based on mass conservation of chemical species, the partial differential equation can be written as (Bear, 1972; Zhao et al., 2008a)

$$\begin{aligned}\frac{\partial(\phi C)}{\partial t} = {} & \frac{\partial}{\partial x}\left(\phi D_{xx}\frac{\partial C}{\partial x} + \phi D_{xy}\frac{\partial C}{\partial y} - \phi V_x\right) \\ & + \frac{\partial}{\partial y}\left(\phi D_{yx}\frac{\partial C}{\partial x} + \phi D_{yy}\frac{\partial C}{\partial y} - \phi V_y\right) \\ & + \rho_s \Gamma \cdot 6 \cdot n^{1/3}(\phi_f - \phi)^{2/3}(C - C_{eq})\end{aligned} \tag{4}$$

where V_x and V_x are the components of the average linear velocity in the x and y directions [LT^{-1}]; D_{xx}, D_{xy}, D_{yx} and D_{yy} are the components of hydrodynamic dispersion coefficient tensor, which are expressed as

$$D_{xx}(x,y) = a_L\frac{V_x(x,y)^2}{|V(x,y)|} + a_T\frac{V_y(x,y)^2}{|V(x,y)|} + D_m(\phi) \tag{5a}$$

$$D_{xy}(x,y) = D_{yx}(x,y) = (a_L - a_T)\frac{V_x(x,y)\cdot V_y(x,y)}{|V(x,y)|} \tag{5b}$$

$$D_{yy}(x,y) = a_L\frac{V_y(x,y)^2}{|V(x,y)|} + a_T\frac{V_x(x,y)^2}{|V(x,y)|} + D_m(\phi) \tag{5c}$$

where a_L and a_T are the longitudinal and transverse dispersivities [L]; ρ_s represents the solid molar density of soluble mineral [ML^{-3}]; $D_m(\phi)$ denotes the porosity dependent molecular diffusion coefficient [L^2T^{-1}]. The common phenomenological relation for $D_m(\phi)$ is (Bear, 1972; Lerman, 1979)

$$D_m(\phi) = D_i\phi^M \quad \frac{3}{2} < M < \frac{5}{2} \tag{6}$$

where D_i is the solute diffusion coefficient [L^2T^{-1}].

For the two-dimensional dissolution front benchmark problem, a rectangular domain and the groundwater initially flowing from the left boundary to the right boundary (along x direction) was usually considered in several study (Chadam et al., 1986; Chen and Liu, 2002, 2004; Zhao et al., 2008a,b). Moreover, based on our previous investigation (Chen and Liu, 2002, 2004) the y component of the average linear velocity was markedly smaller than the y component of the average linear velocity. Accordingly we can assume $V_x \gg V_y$ and the Eqs. (5a)–(5c) can be further simplified as

$$D_{xx}(x,y) = a_L|V_x(x,y)| + D_m(\phi) \tag{7a}$$

$$D_{xy}(x,y) = D_{yx}(x,y) = 0 \tag{7b}$$

$$D_{yy}(x,y) = a_T|V_x(x,y)| + D_m(\phi) \tag{7c}$$

Applying Darcy's law, the x components of average linear velocity can be determined as

$$V_x(x,y) = -\frac{1}{\phi}\psi(\phi)\frac{\partial p}{\partial x} \tag{8}$$

Substituting Eqs. (1), (7a)–(7c) and (8) into Eq. (4), we obtain

$$\begin{aligned}\frac{\partial(\phi C)}{\partial t} = {}& \frac{\partial}{\partial x}\left[\left(a_L\left|\psi(\phi)\frac{\partial p}{\partial x}\right| + \phi D_m(\phi)\right)\frac{\partial C}{\partial x} + \psi(\phi)\frac{\partial p}{\partial x}C\right] \\ & + \frac{\partial}{\partial y}\left[\left(a_T\left|\psi(\phi)\frac{\partial p}{\partial x}\right| + \phi D_m(\phi)\right)\frac{\partial C}{\partial y} + \psi(\phi)\frac{\partial p}{\partial y}C\right] \\ & + 6\rho_s\Gamma n^{1/3}(\phi_f - \phi)^{2/3}(C_{eq} - C)\end{aligned} \tag{9}$$

Dimensionless variables and governing equations are always preferred in the study of problems involving multiple scales and multiple processes (Zhao et al., 2008a). For this reason, we use dimensionless variables and the associated governing equations in the following development of our numerical model.

In most geochemical systems consisting of reactive minerals, the solid molar density of a soluble mineral greatly exceeds the corresponding equilibrium concentration of the soluble mineral; thus a small parameter can be defined as follows:

$$\varepsilon = \frac{C_{eq}}{\rho_s} \ll 1 \tag{10}$$

Defining the following dimensionless variables:

$$\overline{C} = \frac{C}{C_{eq}}, \quad \overline{p} = \frac{\psi(\phi_f)}{\phi_f D_m(\phi_f)}p, \quad \overline{t} = \Gamma\cdot 6n^{1/3}C_{eq}\varepsilon\cdot t,$$

$$\overline{x} = \sqrt{\frac{\Gamma\cdot 6n^{1/3}C_{eq}}{\phi_f D_m(\phi_f)}}x, \quad \overline{y} = \sqrt{\frac{\Gamma\cdot 6n^{1/3}C_{eq}}{\phi_f D_m(\phi_f)}}y.$$

and inserting these dimensionless variables into Eqs. (1), (2), and (9), we obtain the following dimensionless governing equations:

$$\varepsilon\frac{\partial\phi}{\partial\overline{t}} = (\phi_f - \phi)^{2/3}(1 - \overline{C}) \tag{11}$$

$$\varepsilon\frac{\partial\phi}{\partial\overline{t}} = \frac{\partial}{\partial\overline{x}}\left[\overline{\psi}(\phi)\frac{\partial\overline{p}}{\partial\overline{x}}\right] + \frac{\partial}{\partial y}\left[\overline{\psi}(\phi)\frac{\partial\overline{p}}{\partial\overline{y}}\right] \tag{12}$$

$$\begin{aligned}\varepsilon\frac{\partial(\phi\overline{C})}{\partial\overline{t}} = {}& \frac{\partial}{\partial\overline{x}}\left[\left(\overline{a_L}\overline{\psi}(\phi)\frac{\partial\overline{p}}{\partial\overline{x}} + \overline{D_m}(\phi)\right)\frac{\partial\overline{C}}{\partial\overline{x}} + \overline{\psi}(\phi)\frac{\partial\overline{p}}{\partial\overline{x}}\overline{C}\right] \\ & + \frac{\partial}{\partial\overline{y}}\left[\left(\overline{a_T}\overline{\psi}(\phi)\frac{\partial\overline{p}}{\partial\overline{x}} + \overline{D_m}(\phi)\right)\frac{\partial\overline{C}}{\partial\overline{y}} + \overline{\psi}(\phi)\frac{\partial\overline{p}}{\partial\overline{y}}\overline{C}\right] \\ & + \frac{1}{\varepsilon}(\phi_f - \phi)^{2/3}(1 - \overline{C})\end{aligned} \tag{13}$$

where $\overline{\psi}(\phi) = \frac{\psi(\phi)}{\psi(\phi_f)}$; $\overline{D_m}(\phi) = \frac{\phi D_m(\phi)}{\phi_f D_m(\phi_f)}$; $\overline{a_L} = \sqrt{\frac{\Gamma\cdot 6\cdot n^{1/3}C_{eq}}{\phi_f D_m(\phi_f)}}a_L$; and $\overline{a_T} = \sqrt{\frac{\Gamma\cdot 6\cdot n^{1/3}C_{eq}}{\phi_f D_m(\phi_f)}}a_T$.

Eqs. (11)–(13) are a set of coupled nonlinear differential equations. A number of numerical techniques have been proposed to solve such coupled nonlinear differential equations. The most rigorous approach is to solve the entire set of coupled differential equations simultaneously. Such an approach is commonly referred to as the fully coupled method (Steefel and Lasaga, 1994). The fully coupled technique requires a global coefficient matrix that includes all the unknown degrees of freedom associated with the discretized problems of the system. However, for most two-dimensional coupled differential equation problems, the fully coupled solver is computationally expensive. In contrast, in the sequential iteration approach (SIA), each of the coupled nonlinear differential equation is solved individually in a sequential manner, thus greatly reducing the size of the coefficient matrix. Yeh and Tripathi (1989) have compared the explicit and implicit SIA and noted that the implicit SIA has a faster convergence. Accordingly, the implicit SIA algorithm is adopted in this study to solve the coupled nonlinear Eqs. (7)–(9). The details of the solution have been demonstrated by Chen and Liu (2002).

Results and discussion

The developed numerical model is applied in order to assess how and to what degree mechanical dispersion influences the morphological patterns of a chemical dissolution front within fluid-saturated porous medium. We consider a two-dimensional chemical dissolution front benchmark problem which has a rectangular domain with the dimensionless length of $\overline{L_x}$ and the dimensionless width of $2\overline{L_y}$ (see Fig. 1). For this two-dimensional benchmark problem, the negative dimensionless pore-water pressure gradient

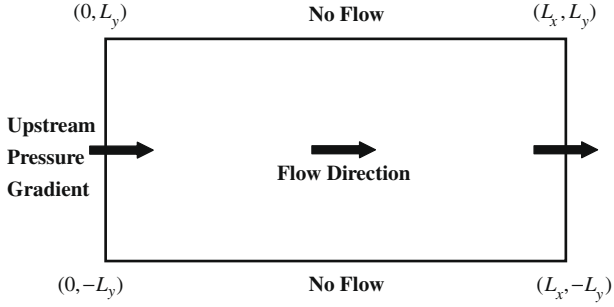

Fig. 1. Schematic diagram of the two-dimensional chemical dissolution front benchmark problem. Groundwater flows from the left-side boundary to the right-side boundary.

is generally applied on the left boundary, implying that the groundwater flows from the left boundary to the right boundary. Accordingly, the left boundary condition for dimensionless pore-water pressure is specified as follows:

$$\frac{\partial \overline{p}}{\partial \overline{x}} = -\overline{p_f} \quad (\overline{x} = 0) \tag{14}$$

where $\overline{p_f}$ denotes a dimensionless pressure gradient imposed on the inlet boundary (referred to as the upstream pressure gradient herein). The upstream pressure gradient is a major factor for determining the patterns of a chemical dissolution front (Chadam et al., 1986; Chen and Liu, 2002, 2004; Zhao et al., 2008a).

Only the net pressure gradient across the region of interest is important since the fluid density in this study is assumed to be a constant. Accordingly, a referenced pressure is prescribed on the right boundary as

$$\overline{p} = 0 \quad (\overline{x} = \overline{L_x}) \tag{15}$$

No flow conditions are used for the upper and lower boundaries and can be expressed as

$$\frac{\partial \overline{p}}{\partial \overline{y}} = 0 \quad (\overline{y} = 0) \tag{16}$$

$$\frac{\partial \overline{p}}{\partial \overline{y}} = 0 \quad (\overline{y} = \overline{L_y}) \tag{17}$$

The boundary condition on the left-side for dimensionless concentration is assigned to be zero

$$\overline{C} = 0 \quad (\overline{x} = 0) \tag{18}$$

The right, upper, and lower boundary conditions for dimensionless concentrations are, respectively, as

$$\frac{\partial \overline{C}}{\partial \overline{x}} = 0 \quad (\overline{x} = \overline{L_x}) \tag{19}$$

$$\frac{\partial \overline{C}}{\partial \overline{y}} = 0 \quad (\overline{y} = 0) \tag{20}$$

$$\frac{\partial \overline{C}}{\partial \overline{y}} = 0 \quad (\overline{y} = \overline{L_y}) \tag{21}$$

Two cases are considered to illustrate the impact of mechanical dispersion on the morphological pattern of chemical dissolution front. The first case is a problem where a single local non-uniformity exists within a homogeneous porous medium, while in the second case we consider a system which is homogeneous everywhere except for two local non-uniformities in the simulation domain.

Case I. A single local non-uniformity

In the case with the single local non-uniformity, the porous medium is homogeneous throughout the simulation area, except a local zone of higher porosity perturbed at the center of the inlet boundary, as shown in Fig. 2. The following initial conditions for the dimensionless porosity and concentration are considered (Chadam et al., 1986; Chen and Liu, 2002)

$$\phi(\overline{x}, \overline{y}, \overline{t} = 0) = \phi_0 + (\phi_f - \phi_0)e^{-\xi} \tag{22}$$

$$\overline{C}(\overline{x}, \overline{y}, \overline{t} = 0) = (1 - e^{-5\overline{x}})(1 - e^{-\xi}) \tag{23}$$

with

$$\xi(\overline{x}, \overline{y}) = (\overline{x}^4 + \overline{y}^4)/(wL_y)^4. \tag{24}$$

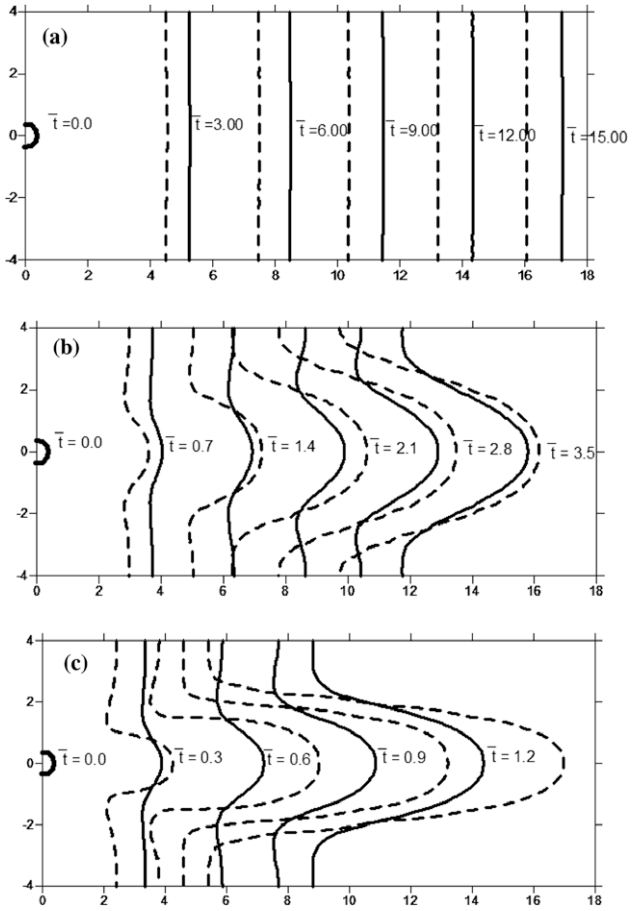

Fig. 2. Temporal evolution of medium porosity contour $\left(\frac{\phi_0+\phi_f}{2}\right)$ for porous medium with a single local non-uniformity under (a) upstream pressure gradient of 0.5; (b) upstream pressure gradient of 2.0; and (c) upstream pressure gradient of 5.0. Solid line: with considering mechanical dispersion, dashed line: without considering mechanical dispersion. The displayed contour is 0.15.

where w is an initial perturbation parameter which is used to perturb the initial local non-uniformity. Eqs. (20)–(24) indicate that the center of the single non-uniformity is located at $(\overline{x} = 0, \overline{y} = 0)$.

It has been indicated in previous studies that the morphological development of a single local non-uniformity without considering mechanical dispersion (Chadam, 1986; Chen and Liu, 2002) is inhibited into a stable planar front when the upstream pressure gradient is smaller than a critical value (referred to as the critical upstream pressure gradient), whereas it evolves into an unstable single-fingering front when upstream pressure gradient is greater than this critical value.

The input parameters used to simulate the morphological evolution of a single local non-uniformity are that initial porosity $\phi_0 = 0.1$; final porosity $\phi_f = 0.2$; dimensionless length $\overline{L_x} = 18$; dimensionless width $\overline{L_y} = 8$; dimensionless longitudinal dispersivity $\overline{a_L} = 1.0$; dimensionless transverse dispersivity $\overline{a_T} = 0.1$; porosity dependent permeability constant $E_1 = 1.0$; porosity dependent diffusion constant $M = 2.0$; initial perturbation parameter $w = 0.1$; the ratio of the equilibrium concentration of the chemical species to the solid molar density of the mineral $\varepsilon = 5 \times 10^{-2}$. The grid sizes for the dimensionless $\overline{x}$ and $\overline{y}$ and the dimensionless time step $\overline{t}$ are 0.1, 0.1, and 0.001. For the condition without mechanical dispersion the dimensionless longitudinal and transverse dispersivities are both set to be zero. It should be noted that the ε value may range from 10^{-3} to 10^{-9} in typical rock (Chadam et al., 1986). This value is at least an order of magnitude greater than

the value of ε (10^{-3}–10^{-9}) in typical rock. The value of ε significantly influences the time step in the numerical simulation. The time step should be reduced as the value of ε decreases, thus leading to a large increase of the computational time. For the case of $\varepsilon = 5 \times 10^{-3}$ the time step needs to be reduced to 1×10^{-5} which is a two orders of magnitude smaller than that for $\varepsilon = 1 \times 10^{-3}$. Accordingly, the value of $\varepsilon = 5 \times 10^{-2}$ is considered herein because more than 100 numerical simulation sets are performed to construct the behavior diagram and the computational loading is intensive.

Fig. 2 displays a comparison between the temporal evolution of porosity contours (with and without considering mechanical dispersion) under different upstream pressure gradients $\overline{p_f}$ of 0.5, 2.0, and 5.0. The solid and dash lines denote the medium porosity iso-line of $\frac{\phi_0+\phi_f}{2} = 0.15$ with and without considering mechanical dispersion, respectively. It is observed that mechanical dispersion retains a stable planar front in shape but accelerates its advancement when $\overline{p_f} = 0.5$ (Fig. 2a). Moreover, mechanical dispersion smears the shape of the unstable single-fingering front and retards the front advancement for $\overline{p_f} = 2.0$ and 5.0 (Figs. 2b and c). The smeared-shape fingering front is a direct consequence of mechanical dispersion which contributes additional elongation-inhibiting mechanism to suppress the chemical dissolution-induced flow-focusing mechanism. We are also interested in seeing if the critical upstream pressure gradient for a planar front is affected by mechanical dispersion. The results of a series of numerical simulations show that mechanical dispersion does not obviously affect the critical upstream pressure gradient for planar front development.

Case II. Two local non-uniformities

The case of two local non-uniformities stands for a homogeneous porous medium with two local zones of higher porosity. The two local non-uniformities are situated at the left boundary of the system, as depicted in Fig. 3. The initial conditions for the dimensionless porosity and concentration are described as follows:

$$\phi(\overline{x},\overline{y},\overline{t}=0) = \phi_0 + (\phi_f - \phi_0)e^{-\xi_1} + (\phi_f - \phi_0)e^{-\xi_2} \tag{25}$$

$$\overline{C}(\overline{x},\overline{y},\overline{t}=0) = (1 - e^{-5\overline{x}})(1 - e^{-\xi_1} - e^{-\xi_2}) \tag{26}$$

where

$$\xi_1(\overline{x},\overline{y}) = [\overline{x}^4 + (\overline{y} - a)^4]/(w\overline{L_y})^4 \tag{27}$$

$$\xi_2(\overline{x},\overline{y}) = [\overline{x}^4 + (\overline{y} + a)^4]/(wL_y)^4 \tag{28}$$

Eqs. (27) and (28) indicate the locations of the two local non-uniformities. The coordinates for the two local non-uniformities are ($\overline{x} = 0$, $\overline{y} = a$) and ($\overline{x} = 0$, $\overline{y} = -a$), respectively. The spacing between the centers of these two non-uniformities (which we refer to as non-uniformity spacing) is $2a$. Chen and Liu (2004) simulated the morphological evolution of two non-uniformities without considering the effect of mechanical dispersion. Their simulation results demonstrated that the two non-uniformities would develop into a stable planar front under a low upstream pressure gradient, but evolve into an unstable single-fingering or double-fingering front under a high upstream pressure gradient. Chen and Liu (2004) further concluded that there are two primary factors, the upstream pressure gradient and non-uniformity spacing, governing the developments of the unstable fingering front in a fluid-saturated porous medium with two local non-uniformities. The double-fingering front develops under a higher upstream pressure gradient; otherwise the single-fingering front emerges. If the upstream pressure gradient is fixed, the single-fingering front develops where there is small non-uniformity spacing; while the

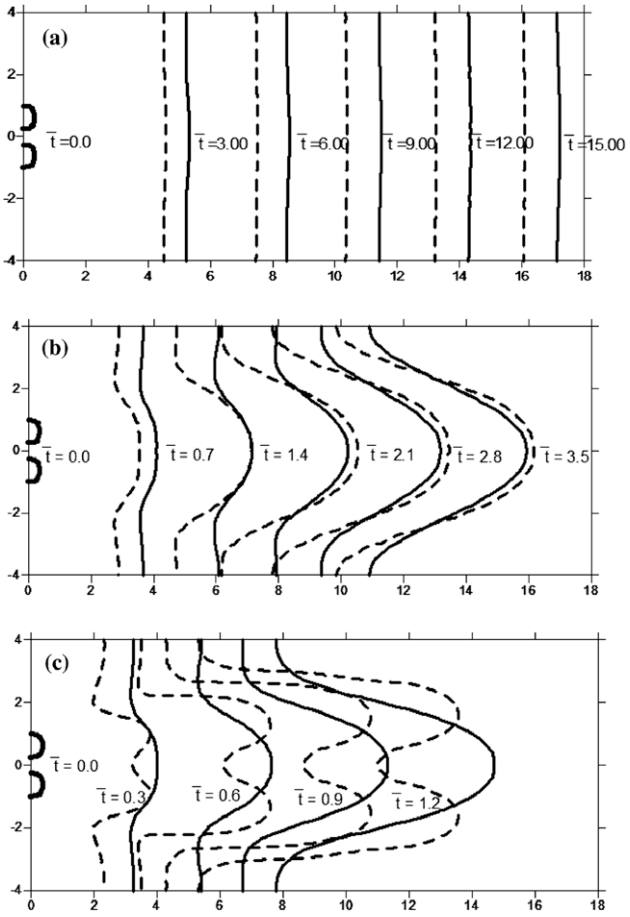

Fig. 3. Temporal evolution of medium porosity contour $\left(\frac{\phi_0+\phi_f}{2}\right)$ for porous medium with two local non-uniformities under (a) upstream pressure gradient of 0.5; (b) upstream pressure gradient of 2.0; and (c) upstream pressure gradient of 5.0 for a fixed spacing of 1.25. Solid line: with considering mechanical dispersion, dashed line: without considering mechanical dispersion. The displayed contour is 0.15.

double-fingering front is maintained where there is larger non-uniformity spacing. Chen and Liu (2004) used primary and secondary critical upstream pressure gradients to explain the aforementioned phenomena. Basically, at a fixed non-uniformity spacing, the unstable single- or double-fingering front, correspond to the upstream pressure gradient exceeding the primary critical upstream pressure gradient value (when the value is below the primary critical upstream pressure gradient, a stable planar front forms). In other words in physical sense the feedback-induced flow-focusing mechanism prevails over the molecular diffusion-induced elongation-inhibiting effect. The unstable double-fingering front further implies that the upstream pressure gradient exceeds the secondary critical upstream pressure gradient value (when the value is below the secondary critical upstream pressure gradient and above the primary critical upstream pressure gradient, an unstable single-fingering front develops; when the value is above both the primary and secondary critical upstream pressure gradients, an unstable double-fingering front evolves). In other words in physical sense the flow-focusing mechanism predominates over the finger-merging effect and elongation-inhibition driven by molecular diffusion. Moreover, Chen and Liu (2004) have constructed a behavior diagram of the dissolution front morphology to characterize the dependence of the primary and secondary critical upstream pressure gradient values on the non-uniformity spacing. The behavior diagram shows that varying non-uniformity spacing does not modify the primary critical upstream pressure gradient value but

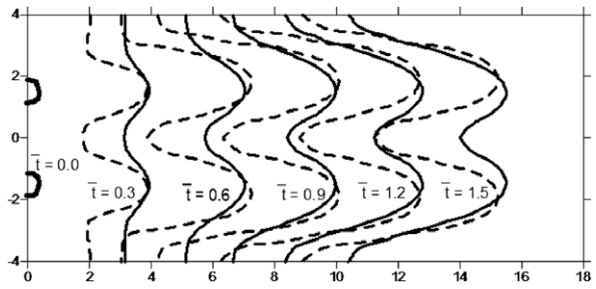

Fig. 4. Temporal evolution of medium porosity contour $\left(\frac{\phi_0+\phi_f}{2}\right)$ for porous medium with two local non-uniformities under upstream pressure gradient of 5.0 for a fixed spacing of 3.0. Solid line: with considering mechanical dispersion, dashed line: without considering mechanical dispersion. The displayed contour is 0.15.

does changes the secondary critical upstream pressure gradient value. Increasing the non-uniformity spacing decreases the value of the secondary critical upstream pressure gradient value.

Fig. 3 presents a comparison between the temporal evolution of porosity contours with and without considering mechanical dispersion under various upstream pressure gradients $\overline{p_f}$ of 0.5, 2.0, and 5.0 but fixing non-uniformity spacing at $2a = 1.25$. It is found that a stable planar front with higher advancement velocity develops for a $\overline{p_f}$ of 0.5 (Fig. 3a). Mechanical dispersion enhances the mixing of reactive solute spatially and accelerates the movement of the stable front. Mechanical dispersion retains the shape of an unstable single-fingering front but significantly shortens the elongation of the single-fingering front for a $\overline{p_f}$ of 2.0 (Fig. 3b). At first, mechanical dispersion initially merges two non-uniformities into a single-fingering front and accelerates the front advancement speed. Later on, the spreading caused by the dispersion at the tip of the front slows the front advancement and the flow-focusing force prevails over the finger-inhibiting mechanism. In the end, the effect of mechanical dispersion on the shape and the chemical dissolution front advancement becomes smothered and slower than that in cases without dispersion. Under higher upstream pressure gradient, mechanical dispersion is enough to merge a double-fingering front into a single-fingering front for a $\overline{p_f}$ of 5.0 (Fig. 3c). This is due to the finger-merging caused by mechanical dispersion prevailing over the flow-focusing process. However, if the non-uniformity spacing is large enough, the double-fingering front may be preserved during the dissolution front development. To further illustrate the physical–chemical process of mechanical dispersion on the morphological evolution of two non-uniformities, we can look at Fig. 4, which shows a comparison of the temporal evolution of porosity contours with and without mechanical dispersion. The fixed upstream pressure gradient $\overline{p_f}$ is 5.0 and the non-uniformity spacing increases to $2a = 3.0$. In this case, mechanical dispersion does not afford to cause the merging of the unstable double-fingering front into an unstable single-fingering front but reduces compresses the finger length of the unstable double-fingering front.

A behavior diagram of the dissolution front morphology is an efficient tool to illustrate the morphological development criteria of two local non-uniformities under various combinations of upstream pressure gradient and non-uniformity spacing. Accordingly, we construct a behavior diagram of the chemical dissolution front with considering the mechanical dispersion. We perform a series of numerical simulations with varying non-uniformity spacing and upstream gradient. In this behavior diagram the upstream pressure gradient is on the abscissa and the non-uniformity spacing is on the ordinate. The reconstructed behavior diagram is then compared with the behavior diagrams without considering mechanical dispersion (Fig. 5). It can be observed that the mechanical dispersion does not alter the primary critical upstream pressure gradient values but raises the secondary critical upstream pressure gradient value for a given non-uniformity spacing. The critical dimensionless pressure gradient for a stable planar front is approximately 0.75. We have compared this value with the result from theoretical analysis of linear stability (Zhao et al., 2008a). Zhao et al. (2008) derived an expression for critical dimensionless upstream pressure gradient as

$$\overline{p_f}\big|_{critical} = -\frac{(3-\beta)(1+\beta)}{2(1-\beta)} \tag{29}$$

where $\beta = \frac{\psi(\phi_0)}{\psi(\phi_f)} = \frac{k(\phi_0)}{k(\phi_f)}$.

Using Eq. (29) the value of critical dimensionless pressure gradient is computed as 1.52. The difference of the critical dimensionless pressure gradient is attributed to that Eq. (25) is obtained by assuming that ε approaches zero which is a special case of morphological evolution of dissolution front.

The double-fingering front occurs under condition of a higher upstream pressure gradient and larger non-uniformity spacing. Moreover, the double-fingering front zone in the behavior diagram is significantly reduced due to the mixing caused by mechanical dispersion.

In summary, mechanical dispersion enhances the fingering-inhibition and/or fingering-merging mechanisms so as to compete with the feedback-inducing flow-focusing mechanism, resulting in

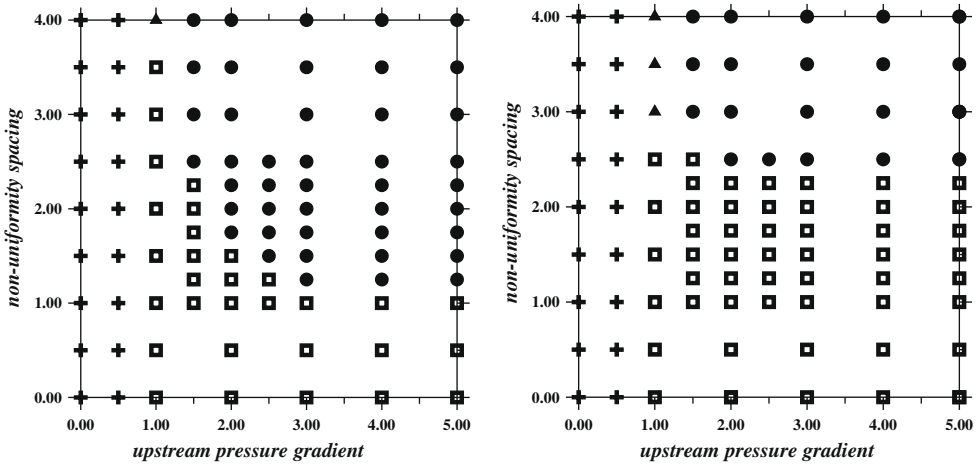

Fig. 5. A comparison of behavior diagrams with and without considering mechanical dispersion (+: stable planar front, ▲: transition zone, □: single-fingering front, ●: double-fingering front).

altering the morphological patterns of the chemical dissolution front and significantly modifying the behavior diagram developed in our previous study (Chen and Liu, 2004).

Conclusions

Mechanical dispersion process plays an important role during species transport within a fluid-saturated porous medium. However, previous studies on the morphological evolution of chemical dissolution front mostly exclude mechanical dispersion. This study expands on our previous work (Chen and Liu, 2004) by incorporating mechanical dispersion into a system of coupled nonlinear governing equations. We rebuild the numerical model to investigate the morphological evolution of a chemical dissolution front affected by mechanical dispersion. Simulation results indicate that mechanical dispersion does not affect the development of stable planar front but prevents elongation of the unstable single-fingering front for a homogeneous porous medium with a single local non-uniformity. For a porous medium with two local non-uniformities, mechanical dispersion can have a variety of effects: (1) the shape of the stable planar front is retained but its advancement is speeded up; (2) the shape of the unstable single-fingering front is retained but the finger length of fingering front is reduced; (3) the unstable double-fingering front merges into an unstable single-fingering front; or (4) the shape of the unstable double-fingering front is preserved but finger length of double-fingering front is reduced. A comparison between behavior diagrams of front morphology (with and without considering mechanical dispersion) shows that the double-fingering front occurs under condition of higher upstream pressure gradient and lager non-uniformity spacing; the zone of the double-fingering front in the behavior diagram is significantly reduced when mechanical dispersion is taken into consideration.

Acknowledgement

The authors would like to thank the National Science Council of the Republic of China for financially supporting this work under Contract No. NSC. 96-2628-M-008-010.

References

Bear, J., 1972. Dynamic of Fluids in Porous Media. Elsevier, Amsterdam. 764pp..
Chadam, J., Hoff, D., Merino, E., Ortoleva, P., Sen, A., 1986. Reactive infiltration instabilities. IMA J. Appl. Math. 36, 207–221.
Chen, J.S., Liu, C.W., 2002. Numerical simulation of the evolution of aquifer porosity and species concentrations during reactive transport. Comput. Geosci. 28, 485–499.
Chen, J.S., Liu, C.W., 2004. Interaction of reactive fronts during transport in a homogeneous porous medium with initial small non-uniformity. J. Contam. Hydrol. 72 (1–4), 47–66.
Chen, W., Ortoleva, P., 1990. Reaction front fingering in carbonate-cemented sandstone. Earth Sci. Rev. 29, 183–198.
Hofner, M.L., Fogler, H.S., 1988. Pore evolution and channel formation during flow and reaction in porous media. AIChE J. 34, 45–54.
Hung, K.M., Hill, A.D., Sepehrnoori, K., 1989. A mechanistic model of wormhole growth in carbonate matrix acidizing and acid fracturing. J. Petrol. Technol. 41 (1), 59–66.
Kalia, N., Balakotaiah, V., 2007. Modeling and analysis of wormhole formation in reactive dissolution of carbonate rocks. Chem. Eng. Sci. 62, 919–928.
Kalia, N., Balakotaiah, V., 2009. Effect of medium heterogeneities on reactive dissolution of carbonates. Chem. Eng. Sci. 64, 376–390.
Lerman, A., 1979. Geochemical Processes. Wiley, New York. 481pp..
Ortoleva, P., 1994. Geochemical Self-organization. Clarendon Press, Oxford. 411pp..
Ortoleva, P., Merino, E., Moor, C., Chadam, J., 1987a. Geochemical self-organization I: feedback mechanisms and modeling approach. Am. J. Sci. 287, 979–1007.
Ortoleva, P., Chadam, J., Merino, E., Sen, A., 1987b. Self-organization in water–rock interaction systems II: the reactive-infiltration instability. Am. J. Sci. 287, 1008–1040.
Renerd, F., Gratier, J.-P., Ortoleva, P., Brosse, E., Bazin, B., 1998. Self-organization during reactive fluid flow in a porous medium. Geophys. Res. Lett. 25 (3), 385–388.
Steefel, C.L., Lasaga, A.C., 1994. A coupled model for transport of multiple chemical species and kinetic precipitation/dissolution reactions with application to reactive flow in single phase hydrothermal systems. Am. J. Sci. 294, 529–592.
Yeh, G.T., Tripathi, V.S., 1989. A critical evaluation of recent developments of hydrogeochemical transport models of reactive multichemical components. Water Resour. Res. 25 (1), 93–108.
Zhao, C., Hobbs, B.E., Hornby, D., Ord, A., Peng, S., Lin, L., 2008a. Theoretical and numerical analyses of chemical-dissolution front instability in fluid-saturated porous rock. Int. J. Numer. Anal. Meth. Geomech. 32, 1107–1130.
Zhao, C., Hobbs, B.E., Ord, A., Hornby, P., Peng, S., 2008b. Effect of reactive surface areas associated with different particles shapes on chemical-dissolution front instability in fluid-saturated porous medium. Transport Porous Med. 73, 75–94.
Zhao, C., Hobbs, B.E., Ord, A., Hornby, P., Peng, S., 2008c. Morphological evolution of three-dimensional chemical dissolution front in fluid-saturated porous media: a numerical simulation approach. Geofluids 8, 113–127.